ELSEVIER

Biochimica et Biophysica Acta 1411 (1999) 101–113

BIOCHIMICA ET BIOPHYSICA ACTA
BBA

# Density functional calculated spin densities and hyperfine couplings for hydrogen bonded 1,4-naphthosemiquinone and phyllosemiquinone anion radicals: a model for the $A_1$ free radical formed in Photosystem I

Patrick J. O'Malley *

*Department of Chemistry, UMIST, Manchester M60 1QD, UK*

Received 27 October 1998; received in revised form 2 February 1999; accepted 11 February 1999

**Abstract**

The B3LYP hybrid density functional method is used to calculate spin densities and hyperfine couplings for the 1,4-naphthosemiquinone anion radical and a model of the phyllosemiquinone anion radical. The effect of hydrogen bonding on the spin density distribution is shown to lead to a redistribution of π spin density from the semiquinone carbonyl oxygens to the carbonyl carbon atoms. The effect of in plane and out of plane hydrogen bonding is examined. Out of plane hydrogen bonding is shown to give rise to a significant delocalisation of spin density on to the hydrogen bond donor heavy atom. Excellent agreement is observed between calculated and experimental hyperfine couplings. Comparison of calculated hyperfine couplings with experimental determinations for the $A_1$ phyllosemiquinone anion radical present in Photosystem I (PS I) of higher plant photosynthesis indicates that the in vivo radical may have a hydrogen bond to the O4 atom only as opposed to hydrogen bonds to each oxygen atom in alcohol solvents. The hydrogen bonding situation appears to be the reverse of that observed for $Q_A$ in the bacterial type II reaction centres where the strong hydrogen bond occurs to the quinone O1 oxygen atom. For different types of reaction centre the presence or absence of the non-heme Fe(II) atom may well determine which type of hydrogen bonding situation prevails at the primary quinone site which in turn may influence the direction of subsequent electron transfer. 

*Keywords:* Photosystem I; $A_1$ free radical; Hyperfine coupling; 1,4-Naphthoquinone; Phylloquinone

## 1. Introduction

Quinones are ubiquitous to living systems. They are key electron transfer intermediates in respiration and photosynthesis [1]. Hydrogen bonding interactions play a key role in anchoring the quinone in the protein site and modifying the redox potential of the quinone for efficient electron transfer [2]. Electron transfer to the quinone results in the formation of the semiquinone anion radical which is amenable to study by electron paramagnetic resonance methods. As a result the plastosemiquinone, phyllosemiquinone and ubisemiquinone anion radicals formed after initial charge separation in higher plant and bacterial photosynthesis have been studied by EPR and ENDOR methods [3–6]. Such methods provide a unique insight into the electronic structure of the radicals and the influence of key hydrogen bonding interactions on electronic structure can be investigated. For biological free radicals the spectra observed are of the powder type, where all orientations

* Fax: +44 (161) 2287040.

0005-2728/99/$ – see front matter 
PII: S0005-2728(99)00036-5

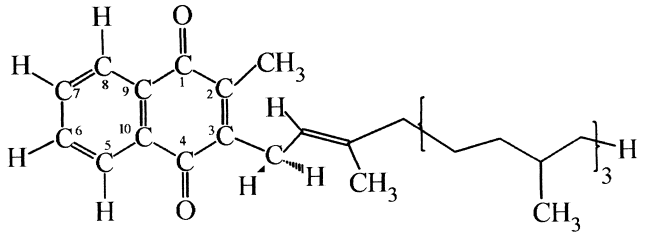

Fig. 1. Phylloquinone (Vitamin K1) molecular structure.

contribute to the radical spectrum. As the anisotropic interactions contribute, the spectra are invariably broadened and of low resolution. Assignment of spectral peaks is difficult and often speculative. Most analyses are confined to $^{1}H$ hyperfine interactions which are an indirect probe of the unpaired electron density. There has been some, but somewhat sparse, success in obtaining $^{17}O$, $^{15}N$ or $^{14}N$ hyperfine couplings for some biological free radicals. Unfortunately $^{13}C$ hyperfines, which would provide the best direct probe of the frontier orbital electron density, provide, often insurmountable, experimental problems and are rarely detected.

We have recently demonstrated the utility of density functional methods for the prediction of hyperfine coupling interactions for semiquinone anion radicals [7–11]. Both isotropic and anisotropic hyperfine couplings can be predicted with impressive accuracy. Prediction of hydrogen bonding hyperfine couplings is also possible. For the electron transfer reactions of photosynthesis, such electronic structure methods can provide us with an accurate electronic structure for the in-transit electron as it visits the various electron transfer pigments. Such information is the key to calculating the electronic contribution to electron transfer. In our previous studies we have calculated the hyperfine couplings for the plastosemiquinone and ubisemiquinone anion radical forms [12,13]. Plastosemiquinone is formed after initial charge separation in Photosystem II whereas ubisemiquinone is formed after initial charge separation in certain purple bacteria. These studies led to reassignments of spectral features and prediction of hydrogen bonding interactions for both semiquinone forms.

In this article we report our findings for a model of the phyllosemiquinone radical, Fig. 1, which is formed after initial charge separation in Photosystem I. From the experimental EPR and ENDOR spectral features observed some tentative assignments were made to methyl group hydrogens and hydrogen bonding protons [6]. Here we calculate the $^{13}C$, $^{17}O$ and $^{1}H$ isotropic and anisotropic hyperfine couplings of the naphthosemiquinone and phyllosemiquinone anion radicals. The effect of symmetrical and asymmetrical hydrogen bonding to the semiquinone carbonyl groups is investigated and rigorous comparison is made with experimental data.

Two recent reports using density functional methods on the properties of fused ring semiquinone anion radicals have appeared [14,15]. These concentrated mainly on the vibrational properties of the free non-hydrogen bonded radicals. Isotropic hyperfine couplings only were calculated for the free radicals and listed but no discussion of the origin or relevance of these couplings was provided nor was the influence of the key hydrogen bonding interactions on the calculated properties discussed.

## 2. Methods

The radicals studied are shown in Figs. 2 and 3. For 1,4-naphthosemiquinone the free non-hydrogen bonded radical, NSQ, was studied in addition to the symmetrical hydrogen bonding situation of two

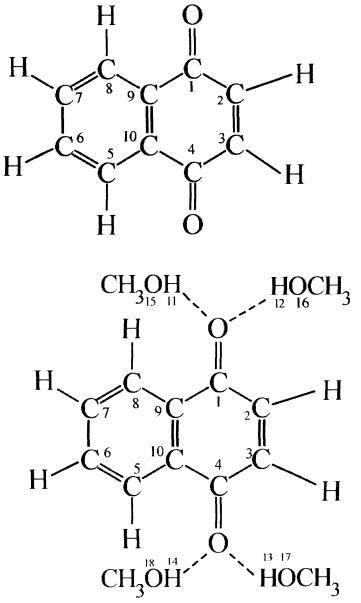

Fig. 2. 1,4-Naphthoquinone (NSQ), top, and its complex with four hydrogen bonding methanol molecules (NSQ-4$CH_3OH$), bottom.

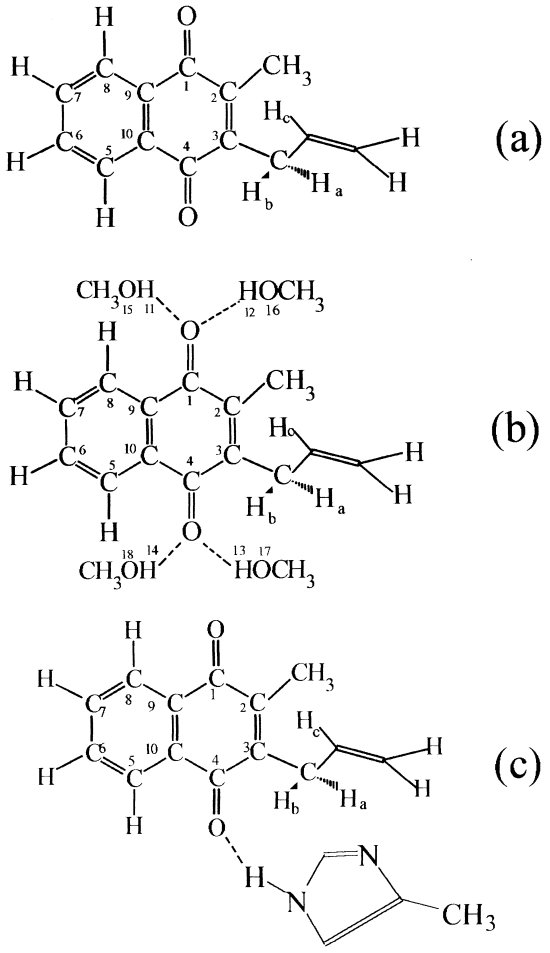


Fig. 3. Models used to study phyllosemiquinone. (a) PHYLLO, (b) PHYLLO-4$CH_3OH$ and (c) PHYLLO-IM. These models illustrate the situation where immobilised hydrogen bonds are formed between the semiquinone and the surrounding methanol molecules in the solid state. In liquid solution a more dynamic hydrogen bonding situation is likely to exist which should be taken into account when comparing calculated values with isotropic values determined in liquid solution.

methanol molecules per each carbonyl, NSQ-4$CH_3OH$, Fig. 2. Naturally occurring phylloquinone (Vitamin $K_1$) has the structure shown in Fig. 1. For computational purposes the phytyl chain at the 3 position has been replaced by a propenyl unit, Fig. 3. Studies on a variety of semiquinones have shown that the length of this chain has no influence on the hyperfine couplings of the radical. For the resultant 2-methyl-3-(propenyl)-1,4-naphthosemiquinone radical the free, PHYLLO, symmetrically hydrogen bonded, PHYLLO-4$CH_3OH$ and the asymmetrical hydrogen bonding situation where the O4 oxygen is hydrogen bonded to methyl imidazole, PHYLLO-IM, were studied, Fig. 3.

For the calculation of spin densities and hyperfine couplings we utilised the B3LYP hybrid functional as implemented on GAUSSIAN94 [16] combined with the EPR-II basis set [17]. The appropriateness of the EPR-II basis set for hyperfine coupling calculations has been recently demonstrated by us [9]. The geometries for the complexes were optimised at the semi-empirical PM3 level using SPARTAN [18] which was also used to generate the spin density surfaces. No symmetry constraints were imposed during the calculations.

## 3. Results and discussion

### 3.1. Naphthosemiquinone

The $^{13}C$ and $^{17}O$ isotropic and anisotropic hyperfine couplings for the NSQ and NSQ-4$CH_3OH$ are given in Table 1. The anisotropic $^{13}C$ and $^{17}O$ hyperfine couplings are directly related to the spin density distribution of the radicals shown in Figs. 4 and 5. Fig. 4 shows that $\pi$ spin density is concentrated on the oxygen atoms. The next region of highest spin is near the C2 and C3 atoms. Appreciable spin is found at the C1/C4 and C9/C10 for the 0.005 e/au$^3$ contour. Spin density is only in evidence at C6/C7 at the wider 0.002 e/au$^3$ contour surface. Most of the changes in the anisotropic hyperfine couplings due to introduction of hydrogen bonding interactions are similar to those reported by us recently for the parent p-benzosemiquinone and durosemiquinone [9–11]. Such hydrogen bonding causes a redistribution of $\pi$ spin density from the carbonyl oxygen atoms to the carbonyl carbon atom positions. This is demonstrated graphically in Fig. 5 and is reflected in the lower absolute anisotropic tensor values for the O1 and O4 atoms and the increased values for the C1 and C4 atom positions in Table 1. The C9 and C10 tensor values are also both reduced quite substantially on hydrogen bond formation. Smaller changes are also observed for the C5, C6, C7 and C8 positions. Most of the tensors in Table 1 are axial indicating that the dominant contribution comes from the $\pi$ spin density at the atom itself. The only exception occurs for the C5 and C8 atom positions. Fig. 4

Table 1
$^{13}C$ and $^{17}O$ calculated anisotropic (T) and isotropic ($A_{iso}$) hyperfine couplings for the 1,4-naphthosemiquinone anion radical complexes of Fig. 2; all values in MHz

| | NSQ | | NSQ-4$CH_3OH$ | |
|---|---|---|---|---|
| | $T_{11}$<br>$T_{22}$<br>$T_{33}$ | $A_{iso}$ | $T_{11}$<br>$T_{22}$<br>$T_{33}$ | $A_{iso}$ |
| O1 | −76.2<br>37.8<br>38.4 | −19.0 | −65.8<br>32.7<br>33.1 | −18.9 |
| O4 | −76.2<br>37.8<br>38.4 | −19.0 | −66.0<br>32.7<br>33.2 | −19.0 |
| C1 | 13.8<br>−5.0<br>−8.8 | −9.6 | 23.1<br>−10.1<br>−13.0 | −3.4 |
| C2 | 17.7<br>−8.6<br>−9.1 | 0.9 | 17.4<br>−8.4<br>−8.9 | −0.3 |
| C3 | 17.7<br>−8.6<br>−9.1 | 0.9 | 17.8<br>−8.6<br>−9.1 | 0.1 |
| C4 | 13.8<br>−5.0<br>−8.8 | −9.6 | 22.7<br>−9.9<br>−12.8 | −3.7 |
| C5 | 1.1<br>0.0<br>−1.1 | −3.8 | 0.7<br>0.2<br>−0.9 | −2.1 |
| C6 | 4.1<br>−1.9<br>−2.2 | 1.4 | 3.7<br>−1.7<br>−2.0 | 0.8 |
| C7 | 4.1<br>−1.9<br>−2.2 | 1.4 | 3.6<br>−1.6<br>−2.0 | 0.7 |
| C8 | 1.1<br>0.0<br>−1.1 | −3.8 | 0.8<br>0.1<br>−0.9 | −2.0 |
| C9 | 8.9<br>−4.2<br>−4.7 | −1.2 | 5.7<br>−2.5<br>−3.2 | −3.5 |
| C10 | 8.9<br>−4.2<br>−4.7 | −1.2 | 5.9<br>−2.6<br>−3.3 | −3.4 |

shows that these are areas of very low π spin density and the contribution to the anisotropic tensor arises principally from the neighbouring spin on the C9/C10 and C6/C7 atoms resulting in a rhombic nature for the tensor values in Table 1. This effect is also in evidence for the C1 and C4 atom tensors of NSQ. For the non-hydrogen bonded case relatively low spin exists at C1 and C4, Fig. 5, and the anisotropic tensor values will have major contributions from the larger spin at the oxygen atoms. On hydrogen bonding more π spin is transferred to the C1 and C4 positions, Fig. 5, which results in a more axial tensor, see Table 1.

The isotropic hyperfine couplings in Table 1 arise from spin density directly at the nuclei in question. As described previously for p-benzosemiquinone [9,10] these couplings arise via spin polarisation effects from the π spin density distribution of the radical operating through the sigma bonds giving rise to finite spin density at the nuclear positions. In summary, taking the π spin of the singly occupied molecular orbital, SOMO, as α, spin polarisation from an atom's own π spin will result in an increase in α spin at that nucleus whereas spin polarisation by a neighbouring π spin will result in an increase in β spin. By convention excess α spin is termed positive spin density whereas excess β spin is negative. The $^{17}O$ isotropic hyperfine coupling remains essentially unchanged on H bonding. The isotropic hyperfine coupling at the C1 and C4 atoms is increased mainly due to the increase in spin at the carbon atoms themselves and also due to the decrease in π spin at the oxygen atoms brought about by hydrogen bond formation. Both of these effects increase the π spin at the carbon nuclei leading to an increased $^{13}C$ isotropic hyperfine coupling. The $^{13}C$ isotropic hyperfine couplings for C2 and C3 decrease on H bonding. As the π spin at these positions remains unchanged on H bond formation this decrease is mainly attributable to the increased π spin at the neighbouring C1 and C4 atoms in the H bonded form. This extra neighbouring π spin leads, via spin polarisation, to more β spin at the C2 and C3 nuclei which explains the decrease in isotropic hyperfine coupling observed. For C6 and C7 a decrease in the isotropic hyperfine coupling is brought about by H bond formation. We attribute this mainly to the decrease in π spin at this position which will reduce the α spin at these nuclei leading to a reduction in the isotropic hyperfine coupling values.

For the C5 and C8 positions which have negligible π spin at their own positions, Fig. 4, the isotropic coupling is principally due to neighbouring atom spin polarisation by π spin at C6/C7 and C9/C10. The decrease in π spin at the C6/C7 and C9/C10

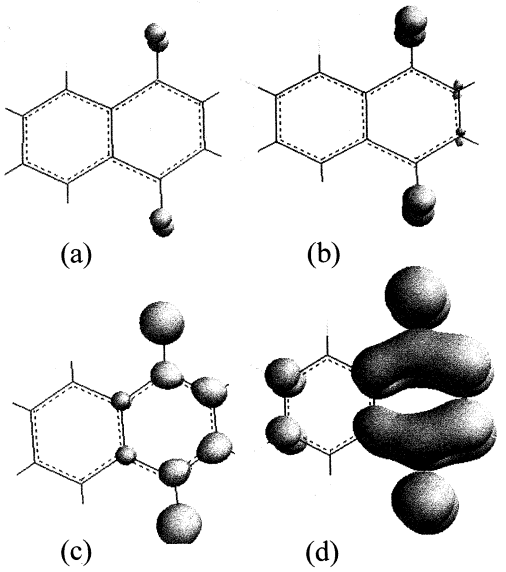


Fig. 4. Positive unpaired spin density contours for NSQ. (a) 0.05 e/au$^3$, (b) 0.015 e/au$^3$, (c) 0.005 e/au$^3$ and (d) 0.002 e/au$^3$. Radical orientation is as given in Fig. 2.

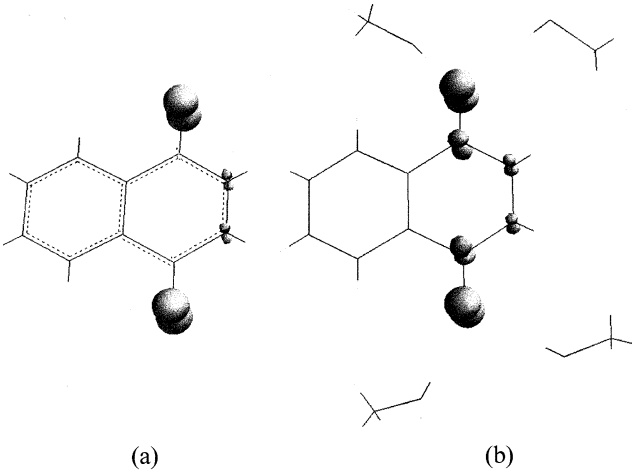


Fig. 5. 0.015 e/au$^3$ positive spin density contours for NSQ (left hand side) and NSQ-4$CH_3OH$ demonstrating increased spin density at the carbonyl carbon atoms on hydrogen bond formation. Radical orientations are as given in Fig. 2.

for NSQ-4$CH_3OH$ therefore results in a decrease in the β spin density at the C5/C8 nuclei which leads to an increased (decreased negative contribution) isotropic hyperfine coupling for these nuclei (−3.8 to −2.1 MHz).

The $^1$H hyperfine couplings are given for NSQ and NSQ-4$CH_3OH$ in Table 2. Some experimental measurements have been obtained in both liquid and solid states [19–21] and these results are also included for comparison with the calculated couplings. Here also the total coupling, A, i.e. isotropic plus anisotropic is given with the isotropic coupling to facilitate comparison with experimental data. The anisotropic coupling for the H atoms arises principally from the dipole-dipole interaction of the H nucleus with the π spin density on the neighbouring carbon atom. The isotropic component is due to spin polarisation of the CH bonding electrons by the π spin on the carbon atom and for positive π spin density at the carbon atom will lead to a negative isotropic hyperfine coupling at the hydrogen atom. The effect of hydrogen bond formation on the calculated hyperfine couplings is less than for the heavy atom data in Table 1. Both the isotropic and anisotropic hyperfine couplings for H2/H3 are similar for NSQ and NSQ-4$CH_3OH$. H6/H7 are also similar in both situations though the lower π spin density at C6 and C7 results in less spin polarisation through the CH bond resulting in a slightly increased (less negative) $^1$H isotropic hyperfine couplings for H6/H7. For H5/H8 the prediction is that the $^1$H isotropic hyperfine coupling is

Table 2
$^1$H total (A) and isotropic ($A_{iso}$) hyperfine couplings calculated for the 1,4-naphthosemiquinone anion radical complexes of Fig. 1; all values given in MHz

| | NSQ | | NSQ-4$CH_3OH$ | | EXPT[a] | |
|---|---|---|---|---|---|---|
| | $A_{11}$ $A_{22}$ $A_{33}$ | $A_{iso}$ | $A_{11}$ $A_{22}$ $A_{33}$ | $A_{iso}$ | $A_{11}$ $A_{22}$ $A_{33}$ | $A_{iso}$ |
| H2 | −1.5 | −8.1 | −1.1 | −8.1 | – | −9.0 |
| | −10.4 | | −10.6 | | −11.4 | |
| | −12.5 | | −12.6 | | −13.4 | |
| H3 | −1.5 | −8.1 | −1.2 | −8.3 | – | −9.0 |
| | −10.4 | | −10.7 | | −11.4 | |
| | −12.5 | | −2.9 | | −13.4 | |
| H5 | −1.9 | 0.0 | −2.6 | −0.8 | – | −1.4 |
| | −0.9 | | −1.2 | | – | |
| | 2.7 | | 1.4 | | – | |
| H6 | −0.2 | −2.2 | 0.1 | −1.9 | – | −1.8 |
| | −2.8 | | −2.6 | | – | |
| | −3.7 | | −3.3 | | – | |
| H7 | −0.2 | −2.2 | 0.1 | −1.9 | – | −1.8 |
| | −2.8 | | −2.5 | | – | |
| | −3.7 | | −3.2 | | – | |
| H8 | −1.9 | 0.0 | −2.6 | −0.8 | – | −1.4 |
| | −0.9 | | −1.2 | | – | |
| | 2.7 | | 1.4 | | – | |

[a]From references [19,21].

zero for the non-hydrogen bonded complex, NSQ. The changes in spin density that take place in the fused ring following hydrogen bond formation, NSQ-4$CH_3OH$, result in a slightly negative value for the isotropic coupling for these atoms, which is in good agreement with experimental TRIPLE resonance measurements, Table 2. On comparing the calculated values with the most recent experimental determinations, Table 2, the agreement is very satisfactory for all isotropic couplings. Anisotropic couplings have only been reported for the H2/H3 positions. Here the two total tensor values reported agree very well with the calculated tensor values as well. These results again emphasise the excellent agreement between hybrid density functional calculated hyperfine couplings and experimental determinations, a point first emphasised by us in references [7,8].

Table 3
$^1H$ and $^{17}O$ anisotropic (T), isotropic ($A_{iso}$) and total (A) calculated hyperfine couplings for the methanol molecules of NSQ-4$CH_3OH$; all values in MHz

| | $T_{11}$ | $A_{iso}$ | $A_{11}$ | EXPT[a] |
|---|---|---|---|---|
| | $T_{22}$ | | $A_{22}$ | |
| | $T_{33}$ | | $A_{33}$ | |
| H11 | 8.5 | −1.3 | 7.2 | – |
| | −4.2 | | −5.5 | −- |
| | −4.3 | | −5.6 | – |
| H12 | 5.9 | 0.2 | 6.1 | 5.6 |
| | −2.8 | | −2.6 | −2.4 |
| | −3.1 | | −2.9 | −2.4 |
| H13 | 5.8 | 0.2 | 6.0 | 5.6 |
| | −2.8 | | −2.6 | −2.4 |
| | −3.1 | | −2.9 | −2.4 |
| H14 | 7.8 | −0.9 | −8.7 | – |
| | −3.8 | | −4.7 | – |
| | −4.0 | | −4.9 | – |
| O15 | −1.3 | −0.9 | −2.2 | – |
| | 0.6 | | −0.3 | – |
| | 0.6 | | −0.3 | – |
| O16 | −0.2 | 0.5 | 0.3 | – |
| | 0.1 | | 0.6 | – |
| | 0.1 | | 0.6 | – |
| O17 | −0.2 | 0.5 | 0.3 | – |
| | −0.1 | | 0.4 | – |
| | 0.1 | | 0.6 | – |
| O18 | −1.0 | −0.7 | −1.7 | – |
| | 0.5 | | −0.2 | – |
| | 0.5 | | −0.2 | – |

[a]From reference [19].

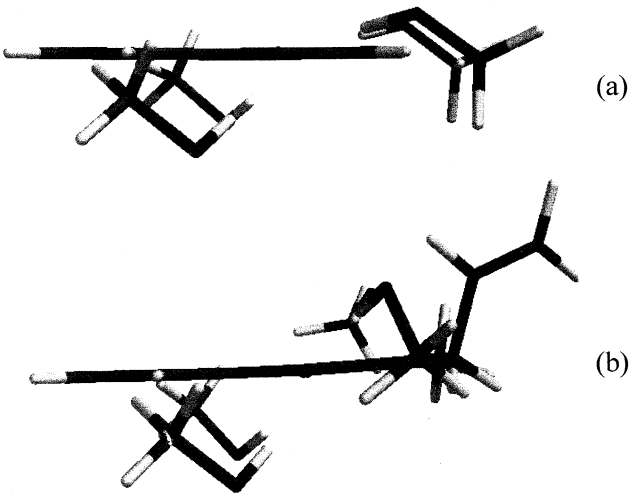


Fig. 6. Side view of minimum energy orientations for the hydrogen bonding methanol molecules in (a) NSQ-4$CH_3OH$ and (b) PHYLLO-4$CH_3OH$.

In Table 3 the hyperfine couplings calculated for the O and hydrogen bonded H atoms of the hydrogen bonding methanol molecules of NSQ-4$CH_3OH$ are collected. To rationalise the data obtained it is instructive to examine the minimum energy orientation located for the hydrogen bonding molecules and this is shown in Fig. 6a. The four hydrogen bonding methanols can be separated into two sets. Two methanol molecules can achieve unrestricted access to the lone pairs on the oxygen atom of the semiquinone and hydrogen bonding lies close to the plane of the semiquinone ring. For the other two molecules the fused ring will not allow in plane hydrogen bonding due to steric effects and the hydrogen bond donor hydrogens are pushed out of the ring plane, Fig. 6a. This is similar to the situation for durosemiquinone [11] where the presence of bulky methyl groups on to the semiquinone oxygen results in an out of plane hydrogen bonding orientation for the hydrogen bond donor group. As for durosemiquinone this results in a negative isotropic hyperfine coupling for the $^1H$ hydrogen bond donors, H11 and H14 in Table 3. The other two hydrogen bond donors are close to the semiquinone ring plane and the classical essentially anisotropic tensor is obtained. Out of plane hydrogen bonding actually leads to a redistribution of spin density from the semiquinone oxygen on to the oxygen atom of the hydrogen bonding methanol molecules. This is demonstrated in Fig. 7 where the

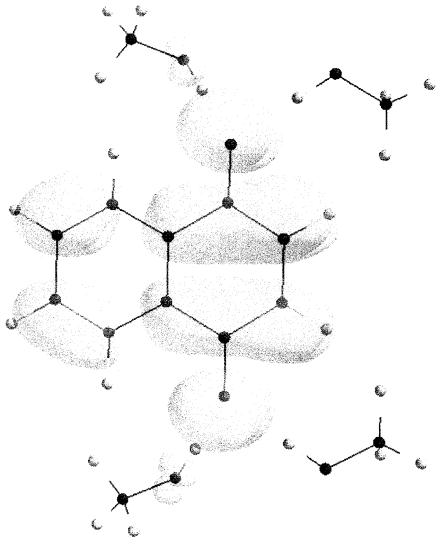

Fig. 7. 0.0002 e/au$^3$ spin density plot contour for NSQ-4$CH_3OH$ demonstrating the presence of positive spin density on the out of plane methanol oxygens.

0.0002 e/au$^3$ contour shows the presence of positive unpaired spin density on the oxygen atoms of the two out of plane methanol molecules while none is observed for the in plane methanol molecules. Spin polarisation of the methanol OH bond electrons by this spin density leads to negative spin at the hydrogen atom nuclei and hence a negative isotropic hyperfine coupling constant for the hydrogen bonding hydrogen. The extra positive spin density on the two out of plane oxygen atoms, O15 and O18, is reflected in their significant absolute anisotropic hyperfine tensor values and the resultant large isotropic hyperfine coupling as well, Table 3. Hyperfine couplings from these hydrogen bonding interactions have been detected experimentally [19] for NSQ in an isopropanol hydrogen bonding solvent and the values obtained are given in Table 3. The values reported are close to that predicted for the in plane hydrogen bonding interaction. As is evident from the durosemiquinone radical spectra, ENDOR spectra for out of plane hydrogen bonds are broadened and less well characterised making them more difficult to detect.

### 3.2. Phyllosemiquinone and $A_1$ model

The $^{13}C$ and $^{17}O$ anisotropic and isotropic hyperfine couplings calculated for the phyllosemiquinone model, PHYLLO, anion radicals of Fig. 3 are presented in Table 4. The changes in hyperfine couplings caused by symmetrical hydrogen bonding are remarkably similar to those described above for the naphthosemiquinone form. Symmetrical hydrogen bonding, PHYLLO-4$CH_3OH$, leads to a redistribution of $\pi$ spin density from the carbonyl oxygen atoms to the carbonyl carbon atoms of the phyllosemiquinone leading to almost identical hyperfine couplings for both radicals as found for the NSQ forms. As for NSQ a decrease in anisotropic hyperfine coupling at the C9/C10 atom positions is also found on hydrogen bond formation. The only noticeable difference in $^{13}C$ anisotropic hyperfine couplings between NSQ and PHYLLO appears to be for the C2 and C3 positions. For NSQ similar anisotropic couplings are observed for these two atoms whereas for the PHYLLO the C3 position has decreased in value somewhat, see Tables 1 and 4. This is likely due to the locked conformation of the propenyl chain which is discussed below. For the asymmetrical hydrogen bonding case, PHYLLO-IM, the changes in spin density distribution and resultant hyperfine couplings are similar to those reported for asymmetrical hydrogen bonding for the durosemiquinone anion radical recently [11]. Hydrogen bond formation to just one oxygen atom i.e. to O4 in this case produces an odd alternant distribution of $\pi$ spin den-

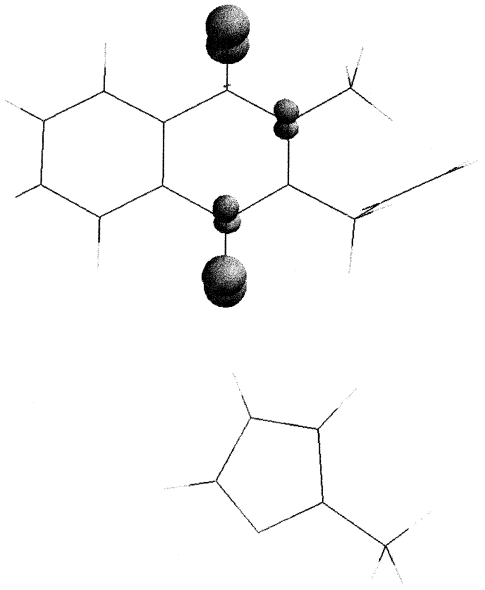

Fig. 8. 0.015 e/au$^3$ positive spin density contour for PHYLLO-IM.

Table 4
$^{13}C$ and $^{17}O$ calculated anisotropic (T) and isotropic ($A_{iso}$) hyperfine couplings for the radical complexes of phyllosemiquinone models in Fig. 3; all values in MHz

| | PHYLLO | | PHYLLO-4$CH_3OH$ | | PHYLLO-IM | |
|---|---|---|---|---|---|---|
| | $T_{11}$ $T_{22}$ $T_{33}$ | $A_{iso}$ | $T_{11}$ $T_{22}$ $T_{33}$ | $A_{iso}$ | $T_{11}$ $T_{22}$ $T_{33}$ | $A_{iso}$ |
| O1 | −76.0 | −19.0 | −61.8 | −17.4 | −78.1 | −19.2 |
| | 37.7 | | 26.4 | | 38.8 | |
| | 38.3 | | 26.1 | | 39.3 | |
| O4 | −73.0 | −18.6 | −59.8 | −17.1 | −64.5 | −18.6 |
| | 36.2 | | 29.7 | | 32.0 | |
| | 36.8 | | 30.1 | | 32.6 | |
| C1 | 15.9 | −9.2 | 26.4 | −1.7 | 13.3 | −11.8 |
| | −6.1 | | −11.9 | | −4.8 | |
| | −9.8 | | −14.5 | | −8.6 | |
| C2 | 18.9 | 2.7 | 17.4 | −0.9 | 23.3 | 6.2 |
| | −9.2 | | −8.4 | | −11.5 | |
| | −9.7 | | −9.0 | | −11.9 | |
| C3 | 15.1 | 0.3 | 14.2 | −1.1 | 10.4 | −4.0 |
| | −7.3 | | −6.8 | | −4.9 | |
| | −7.8 | | −7.4 | | −5.6 | |
| C4 | 16.0 | −8.0 | 26.1 | −0.9 | 23.9 | −1.7 |
| | −6.2 | | −11.8 | | −10.5 | |
| | −9.8 | | −14.4 | | −13.4 | |
| C5 | 1.0 | −3.5 | 0.9 | −2.1 | 0.8 | −1.8 |
| | −0.1 | | −0.1 | | 0.1 | |
| | −1.0 | | −1.0 | | −0.9 | |
| C6 | 4.1 | 1.2 | 4.0 | 0.8 | 2.5 | −0.2 |
| | −1.9 | | −1.8 | | −1.1 | |
| | −2.2 | | −2.2 | | −1.4 | |
| C7 | 3.8 | 1.2 | 3.7 | 0.7 | 5.2 | 2.3 |
| | −1.8 | | −1.7 | | −2.4 | |
| | −2.1 | | −2.0 | | −2.8 | |
| C8 | 1.0 | −3.5 | 1.1 | −2.0 | 1.4 | −4.4 |
| | −0.1 | | 0.0 | | 0.3 | |
| | −0.8 | | −1.1 | | −1.7 | |
| C9 | 8.5 | −1.6 | 5.9 | −4.0 | 9.4 | −0.2 |
| | −4.0 | | −2.6 | | −4.4 | |
| | −4.5 | | −3.3 | | −4.9 | |
| C10 | 8.6 | −1.5 | 6.2 | −3.8 | 6.2 | −4.1 |
| | −4.1 | | −2.8 | | −2.8 | |
| | −4.5 | | −3.4 | | −3.4 | |

sity with spin density being dominant at the C4, C2 and O1 positions. This is graphically demonstrated by the 0.015 e/au$^3$ spin density contour in Fig. 8. The $^{13}C$ anisotropic hyperfine couplings in Table 4 are a direct reflection of this spin density distribution. The absolute magnitude of the O1 tensor values are larger than the O4 ones. The C4 values are increased compared with the C1 values. The C2 values are increased considerably at the expense of much smaller values for C3. An asymmetry is also introduced into the C9 and C10 positions with the C9 showing increased values. The C7 values are increased relative to the C6 position. As described above, the isotropic coupling for each nucleus is determined via spin polarisation by the π spin at its own position and by neighbouring positions. The oxygen atom isotropic couplings for PHYLLO-IM are similar because the spin density contributions at the oxygens themselves (positive) and the carbonyl carbons (negative) cancel. For C1 the lower π spin density at its own position reduces this positive contribution to its isotropic hyperfine coupling and as a result a large negative hyperfine coupling is predicted reflecting spin polarisation from the neighbouring O1 π spin. For C4 the increase in the C4 π spin combined with the decrease in the O4 π spin both contribute positively to its isotropic hyperfine coupling leading to increased values. For the C2 position a substantially increased isotropic hyperfine coupling is predicted mainly due to the increased π spin at this position whereas this high π spin at C2 leads to a negative contribution to the C3 isotropic hyperfine coupling decreasing its value. The larger π spin at C9 also contributes positively to its own isotropic coupling leading to an

Table 5
$^{1}H$ total (A) and isotropic ($A_{iso}$) hyperfine couplings calculated for the phyllosemiquinone anion radical model complexes of Fig. 1; all values given in MHz

| | PHYLLO | | PHYLLO-4$CH_3OH$ | | PHYLLO-IM | |
|---|---|---|---|---|---|---|
| | $T_{11}$ $T_{22}$ $T_{33}$ | $A_{iso}$ | $T_{11}$ $T_{22}$ $T_{33}$ | $A_{iso}$ | $T_{11}$ $T_{22}$ $T_{33}$ | $A_{iso}$ |
| H5 | 2.7 | −0.1 | 2.1 | −0.9 (1.5) | 2.2 | −1.0 |
| | −0.8 | | −0.3 | | −0.4 | |
| | −1.9 | | −1.8 | | −1.8 | |
| H6 | 2.0 | −2.1 | 2.1 | −2.0 (2.0) | 1.7 | −1.3 |
| | −0.6 | | −0.6 | | −0.7 | |
| | −1.4 | | −1.5 | | −1.1 | |
| H7 | 2.0 | −2.1 | 2.1 | −2.0 (2.0) | 2.3 | −2.7 |
| | −0.6 | | −0.7 | | −0.6 | |
| | −1.4 | | −1.4 | | −1.7 | |
| H8 | 2.7 | −0.1 | 2.1 | −0.9 (1.5) | 2.9 | 0.3 |
| | −0.8 | | −0.3 | | −1.0 | |
| | −1.9 | | −1.8 | | −1.9 | |

Experimental *absolute* values from reference [20] given in brackets.

Table 6
$^1$H total (A) and isotropic ($A_{iso}$) calculated hyperfine couplings for the methyl group and phytyl chain protons of the phyllosemiquinone anion radical model complexes in Fig. 3; all values in MHz

| | PHYLLO | | PHYLLO-4$CH_3OH$ | | PHYLLO-IM | | EXPT[a] | |
|---|---|---|---|---|---|---|---|---|
| | $A_{11}$ | $A_{iso}$ | $A_{11}$ | $A_{iso}$ | $A_{11}$ | $A_{iso}$ | $A_{11}$ | $A_{iso}$ |
| | $A_{22}$ | | $A_{22}$ | | $A_{22}$ | | $A_{22}$ | |
| | $A_{33}$ | | $A_{33}$ | | $A_{33}$ | | $A_{33}$ | |
| $CH_3$ (2) | 10.6 | | 10.9 | | 12.6 | | 10.0 (12.6) | |
| | 6.9 | 7.8 | 7.2 | 8.1 | 9.2 | 10.0 | 6.8 (9.0) | 7.9 (10.2) |
| | 5.9 | | 6.3 | | 8.2 | | 6.8 (9.0) | |
| $CH_2$ (3a) | 5.0 | | 6.0 | | 5.5 | | – | |
| | 2.1 | 3.7 | 1.8 | 2.8 | 1.4 | 2.4 | – | 3.6 |
| | 1.3 | | 0.6 | | 0.3 | | – | |
| $CH_2$ (3b) | 6.9 | | 5.2 | | 4.0 | | – | |
| | 2.8 | 2.8 | 2.3 | 3.0 | 1.3 | 1.9 | – | 3.6 |
| | 1.5 | | 1.5 | | 0.5 | | – | |
| CH (3c) | 1.9 | −0.3 | 2.0 | −0.3 | 2.0 | −0.2 | – | 0.3 |
| | −1.2 | | −1.2 | | −1.1 | | – | |
| | −1.6 | | −1.6 | | −1.5 | | – | |

[a]From references [6,19,20]. The experimental values were reported for the in vitro phyllosemiquinone radical in an alcohol solvent. The values reported for the $A_1$ radical of Photosystem I (6) are given in brackets. No signs were given for the experimental values.

increased value. The lower π spin density at C10 leads to a decrease in its isotropic hyperfine coupling value. Increased spin density at C7 again increases its isotropic hyperfine coupling value whereas the lower spin at C6 leads to a corresponding decrease in its isotropic hyperfine coupling value. The C5 isotropic hyperfine coupling is predicted to be increased in value for PHYLLO-IM whereas a decrease in hyperfine coupling is predicted for C8.

The $^1$H data for the 5, 6, 7 and 8 positions of the PHYLLO radical complexes are presented in Table 5. Again the similarity both qualitatively and quantitatively for PHYLLO and PHYLLO-4$CH_3OH$ to NSQ and NSQ-4$CH_3OH$ is striking. The agreement with experimental data for the isotropic couplings is again impressive and the signs of the hyperfine couplings, which have not been experimentally determined, can be reliably given from the calculations here. The spin density asymmetry introduced by one sided hydrogen bonding, PHYLLO-IM, is also reflected in the $^1$H data of Table 5. The higher π spin at the C7 position compared with C6 results in a more negative hyperfine coupling for H7 compared with H6.

The hyperfine couplings for the methyl group at the C2 position and the β and γ protons of the propenyl chain at C3 are presented in Table 6. Experimental values reported for phyllosemiquinone in an alcohol solvent and for the $A_1$ radical of Photosystem I (PS I) are also given for comparison. The agreement between calculated couplings and experimental determinations is excellent. Of particular note is the agreement between the calculated values for the asymmetrical form PHYLLO-IM and the experimentally determined values for the $A_1$ radical of PS I. The position of $A_1$ in the PS I reaction centre cannot be reliably determined from the current X-ray electron density resolution [22]. Recent modelling studies [23] attempted to predict a reaction centre location for the $A_1$ quinone molecule and identify key hydrogen bonding residues; the well resolved $Q_A$ binding sites of the bacterial reaction centres (bRCs) being used as a model. For the $Q_A$ molecule in the *Rps viridis* bacterial reaction centre it is quite well established that a strong hydrogen bond exists between the O1 oxygen atom and M-His-217, which also acts as a ligand to the non-heme Fe(II). We retain the numbering scheme shown in Fig. 1 for

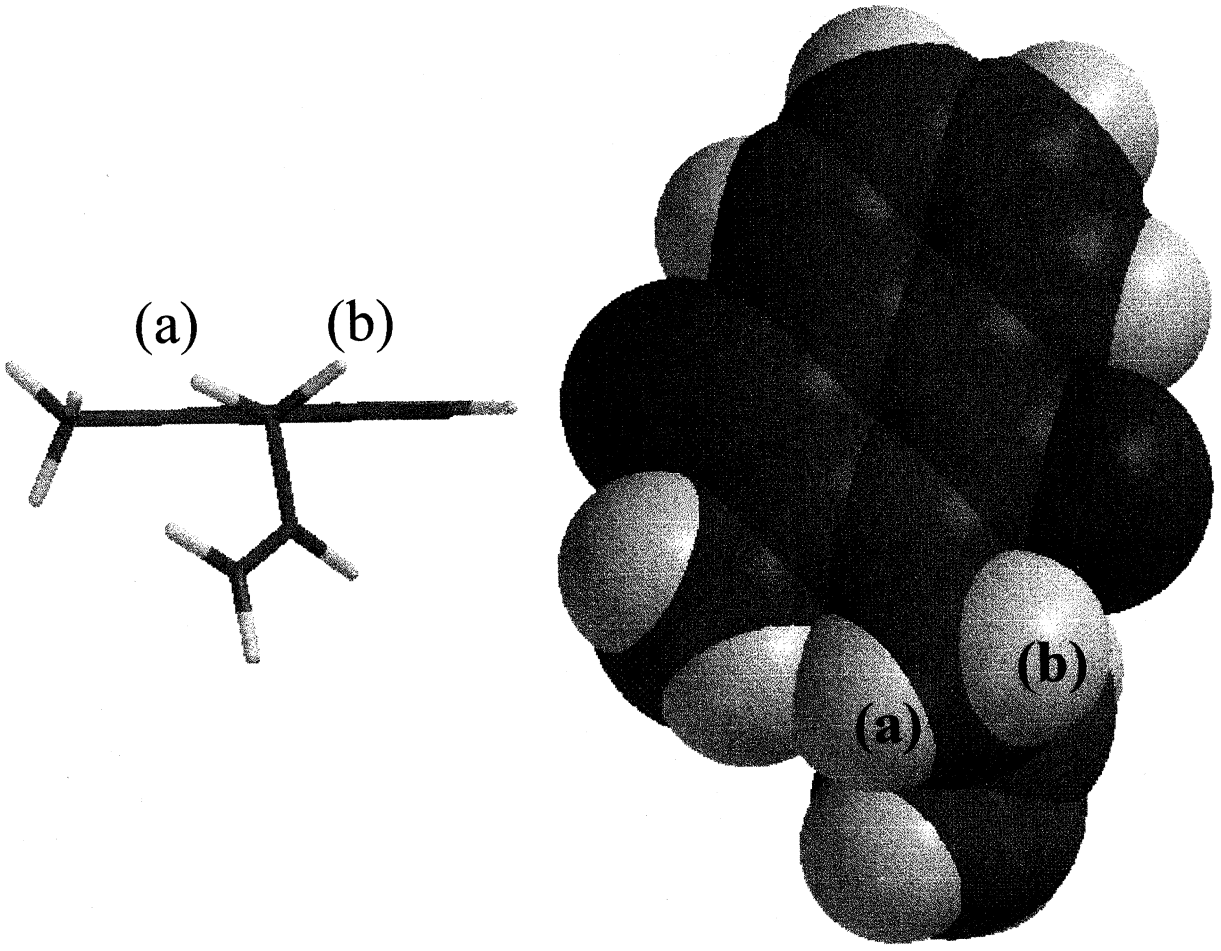


Fig. 9. Side view of optimised geometry of PHYLLO showing the almost perpendicular (86 degrees) orientation of the propenyl chain relative to the quinone ring plane. On right hand side a space filling model, looking down on the quinone plane, demonstrates the steric crowding caused by the presence of the methyl group substituent at C2 which locks the long chain at C3 into this perpendicular orientation.

the menaquinonequinone species, i.e. O4 proximal to the isoprenoid chain. A weaker hydrogen bond forms between the O4 oxygen and the backbone amide group of M-Ala-260. Such a hydrogen bonding situation gives rise to an asymmetric spin density distribution for $Q_A$ caused by the stronger hydrogen bonding to the M-His-217-Fe(II) complex. The positive charge on the histidine-Fe(II) complex has been shown to be responsible for the asymmetry observed [13]. Interestingly the Fe(II) ion is absent in the PS I reaction centre and the modelling studies of reference [23] have concluded that no suitable hydrogen bond donors are present for hydrogen bond donation to the O1 oxygen atom of $A_1$. In our density functional calculations, asymmetric hydrogen bonding to the O1 leads to, in comparison with the symmetric PHYLLO-4$CH_3OH$, reduced methyl group coupling and an enhanced methylene proton coupling (unpublished data) which is in disagreement with the experimental methyl group couplings for $A_1$. Based on the analogy with the bacterial reaction centre the most plausible situation is that, in the absence of a strong hydrogen bond donor to O1, hydrogen bonding to $A_1$ occurs at the O4 atom only, as in our PHYLLO-HIS model. In support of such a model, MacMillan et al. [24] showed that the O-O axis of the $Q_A$ semiquinone in the bRC, needed to be rotated by $\sim 60$ degrees out of the membrane plane to correspond to the $A_1$ orientation in PS I. This required the breaking of the histidine hydrogen bond to O1 while retaining the hydrogen bond to O4. Our recent study [13], which showed the crucial role played by the

Table 7
$^{1}H$ and $^{17}O$ anisotropic (T) and isotropic ($A_{iso}$) calculated hyperfine couplings for the methanol molecules of PHYLLO-4$CH_3OH$; all values in MHz

| | $T_{11}$<br>$T_{22}$<br>$T_{33}$ | $A_{iso}$ |
|---|---|---|
| H11 | 8.3<br>−4.1<br>−4.2 | −1.4 |
| H12 | 7.6<br>−3.6<br>−4.1 | −1.1 |
| H13 | 7.4<br>−3.6<br>−3.8 | −0.9 |
| H14 | 8.4<br>−4.1<br>−4.3 | −1.5 |
| O15 | −1.3<br>0.7<br>0.7 | −1.0 |
| O16 | −1.1<br>0.5<br>0.6 | −0.6 |
| O17 | −1.0<br>0.5<br>0.5 | −0.5 |
| O18 | −1.4<br>0.7<br>0.7 | −1.0 |

non-heme Fe(II) in the strong hydrogen bond to O1 for the bRC, suggests that its presence and associated histidine ligand may be a prerequisite for hydrogen bonding to the O1 oxygen of the primary quinone electron acceptor. The oxygen atoms of the semiquinone carry most of the frontier orbital electron density, Fig. 4, and intriguingly the subsequent electron transfer step appears to correspond to the direction of the O-O axis: primarily along the membrane plane to $Q_B$ for the bRC and mainly perpendicular to the membrane plane to the FeS centres for PS I.

In the model we have chosen an imidazole as our hydrogen bond donor but other hydrogen bond donors, such as an amide NH or hydroxyl group, can be shown to produce essentially identical results to those given in Table 6. Our conclusion therefore is that one sided hydrogen bonding to the O4 oxygen atom occurs for the $A_1$ molecule and this is the cause of the unusually high hyperfine coupling observed experimentally for the methyl group of the $A_1$ radical in PS I [6]. In reference [23] the presence of π-π stacking interactions with a neighbouring tryptophan residue was proposed as a possible origin for the spin asymmetry observed. So far there is no firm evidence either on experimental or theoretical grounds that such interactions have any influence on the spin density distribution of the radical species. The presence of one sided hydrogen bonding could explain two other properties of the $A_1$ species already observed. The $g_{xx}$ value for the $A_1$ radical is significantly larger than that observed for the phyllosemiquinone radical in alcohol solvents [24,25]. This can be explained by the argument that one of the oxygen atoms O1 is free from strong hydrogen bonds in $A_1$. The resultant large spin density on this oxygen will lead to an increased $g_{xx}$ value compared with phyllosemiquinone in alcohol solvents where both oxygens are hydrogen bonded. The $E_m$ value for $A_1$ is also approximately 700 mV lower than that observed for phylloquinone in alcohol solvents [6]. We have recently demonstrated the influence of hydrogen bonding on the electron affinity of p-benzoquinone [2]. Here we showed that increasing the number of hydrogen bonds to the quinone carbonyls led to a substantial increase (approximately 250 meV per hydrogen bond) in the electron affinity of the quinone. We have proposed above that one hydrogen bond exists for $A_1$ to the O4 oxygen as opposed to the expected four for the quinone in an alcohol solvent. Based on the electron affinity alone this will lead to a lowering of the reduction potential by approximately 750 mV compared with the quinone in an alcohol solvent.

The $^{1}H$ hyperfine coupling values for the β and γ proton of the propenyl chain are also given in Table 6. As found experimentally the isotropic coupling for the β protons is about half the value of the coupling for the methyl group protons at the C2 position. Indeed this is a typical scenario for semiquinones where a methyl group exists at the C2 position; other examples include ubisemiquinone and α-tocopherol [20,26]. When the C2 position has a hydrogen substituent e.g. plastosemiquinone, the $^{1}H$ hyperfine coupling for the long chain at C3 is double this value as it is when a methyl group is present at the C3 position. When the C2 position contains a bulky

methyl group the *only* conformation allowed for the long chain is such that the second carbon atom of the chain makes close to a 90 degree dihedral angle with the quinone ring plane, see Fig. 9. In other words the long chain is locked into this conformation. This allows the two β methylene protons to make close to 60 degree angle overlaps with the π orbital lobe on C3. The usual $\cos^2\theta$ dependence for hyperconjugation, where θ is the dihedral angle the protons make with the π orbital lobe at the C3 atom, is therefore approximately 1/4 for these protons as opposed to the 1/2 value for a freely rotating group and explains the apparent halving in hyperfine coupling observed for long chain semiquinones which have a methyl group at the C2 position.

The small isotropic hyperfine coupling determined recently for H3c, in phyllosemiquinone, is again in excellent agreement with the theoretically predicted value, see Table 6.

Table 7 contains the calculated hyperfine couplings for the hydrogen bonding hydrogen and the oxygen atoms of the hydrogen bonded methanol molecules. Fig. 6b shows the optimum configuration taken up by the hydrogen bonding methanols. In contrast to the naphthosemiquinone case all hydrogen bonding positions around the phyllosemiquinone carbonyl oxygens are crowded and only out of plane hydrogen bonding is permitted. This results in methanol oxygen hyperfine tensors characteristic of out of plane hydrogen bonding. π spin density delocalises from the semiquinone carbonyl oxygens to the oxygen atoms of the hydrogen bonding methanols. This results in a significant anisotropic and isotropic hyperfine coupling for all the oxygen atoms of the four methanol molecules and also a negative isotropic hyperfine coupling for the methanol OH hydrogen atoms. It is also of note here that the decrease in the anisotropic hyperfine coupling in going from free to the symmetrical hydrogen bonded case is greater for the phyllosemiquinone model. This is due to the extra transfer of spin density from the semiquinone carbonyl oxygens for phyllosemiquinone, caused by the presence of four out of plane hydrogen bonds as opposed to only two for the naphthosemiquinone. $^1$H hyperfine interactions for phyllosemiquinone in an alcohol solvent and for the $A_1$ radical were detected experimentally in reference [6]. It was assumed however that a purely dipolar interaction accounted for the hydrogen bonding interaction. As is now known however this is not the case for out of plane hydrogen bonding and proper interpretation of the hydrogen bonding data needs to account for this. Clearly further studies need to be performed, with the aid of the theoretical predictions of this paper, to fully assign any experimental hyperfine data associated with hydrogen bonding interactions. As concluded in reference [23] no reliable data can also be inferred from the methylene $^1$H data reported in reference [6].

## 4. Conclusion

Density functional calculated hyperfine couplings for the anion radicals 1,4-naphthoquinone and a model of phylloquinone show excellent agreement with experimental data. The effect of hydrogen bonding on the spin density distribution is shown to lead to a redistribution of π spin density from the semiquinone carbonyl oxygens to the carbonyl carbon atoms. Comparison of calculated hyperfine couplings with experimental determinations for the A1 phyllosemiquinone anion radical present in Photosystem I of higher plant photosynthesis indicates that the in vivo radical may have a strong hydrogen bond to the O4 atom only as opposed to hydrogen bonds to each oxygen atom in alcohol solvents. The hydrogen bonding situation appears to be the reverse of that observed for $Q_A$ in the bacterial type II reaction centres where the strong hydrogen bond occurs to the quinone O1 oxygen atom. The presence or absence of the non-heme Fe(II) atom and associated histidine ligand may well determine which type of hydrogen bonding situation prevails at the primary quinone site.

## References

[1] B.L. Trumpower (Ed.), Functions of Quinones in Energy Conserving Systems, Academic Press, New York, 1986.
[2] P.J. O'Malley, Chem. Phys. Lett. 274 (1997) 251.
[3] G. Feher, R.A. Isaacson, M.Y. Okamura, W. Lubitz, in: M.E. Michel-Beyerle (Ed.), Antennas and Reaction Centers of Photosynthetic Bacteria, Springer-Verlag, Berlin, 1985, pp. 174–189.

[4] F. MacMillan, F. Lendzian, G. Renger, W. Lubitz, Biochemistry 34 (1995) 8144.
[5] S.E.J. Rigby, P. Heathcote, M.C.W. Evans, J.H.A. Nugent, Biochemistry 34 (1995) 12075.
[6] S.E.J. Rigby, P. Heathcote, M.C.W. Evans, Biochemistry 35 (1996) 6651.
[7] S.J. Collins, P.J. O'Malley, Chem. Phys. Lett. 259 (1996) 296.
[8] P.J. O'Malley, Chem. Phys. Lett. 262 (1996) 797.
[9] P.J. O'Malley, J. Phys. Chem. A 101 (1997) 6334.
[10] P.J. O'Malley, Phys. Chem. A 101 (1997) 9813.
[11] P.J. O'Malley, J. Phys. Chem. A 102 (1998) 248.
[12] P.J. O'Malley, J. Am. Chem. Soc. 120 (1998) 5093.
[13] P.J. O'Malley, Chem. Phys. Lett. 285 (1998) 99.
[14] A.K. Grafton, S.E. Boesch, R.A. Wheeler, J. Mol. Struct. (Theochem.) 392 (1997) 1.
[15] A.K. Grafton, R.A. Wheeler, J. Phys. Chem. A 101 (1997) 7154.
[16] M.J. Frisch, G.W. Trucks, H.B. Schlegel, P.W. Gill, B.G. Johnson, M.W. Wong, J.B. Foresman, M.A. Robb, M. Head-Gordon, E.S. Replogle, R. Gomperts, J.L. Andres, K. Raghvachari, J.S. Binkley, C. Gonzalez, R.L. Martin, D.J. Fox, D.J. Defrees, J. Baker, J.J.P. Stewart, J.A. Pople, GAUSSIAN 94, Gaussian Inc., Pittsburgh, PA, 1995.
[17] V. Barone, in: D.P. Chong (Ed.), Recent Advances in Density Functional Methods, World Scientific Publishing, Singapore, 1995.
[18] SPARTAN 4.1.1, Wavefunction Inc., California, 1995.
[19] F. MacMillan, Doctoral Thesis, Freie Universität Berlin, Chemistry Department, 1993.
[20] M.R. Das, H.D. Connor, D.S. Leniart, J.H. Freed, J. Am. Chem. Soc. 92 (1970) 2258.
[21] B. Kirste, Magn. Res. Chem. 25 (1987) 166.
[22] W.-D. Schubert, O. Klukas, N. Krauss, W. Saenger, P. Fromme, H.T. Witt, J. Mol. Biol. 272 (1997) 741.
[23] A. Kamlowski, B. Altenburg-Greulich, A. van der Est, S.G. Zech, R. Bittl, P. Fromme, W. Lubitz, D. Stehlik, J. Phys. Chem. 102 (1998) 8278.
[24] F. MacMillan, J. Hanley, L. van der Weerd, M. Knupling, S. Un, A.W. Rutherford, Biochemistry 36 (1997) 9297.
[25] A. Van der Est, T. Prisner, R. Bittl, P. Fromme, W. Lubitz, K. Mobius, D. Stehlik, J. Phys. Chem. B 101 (1997) 1437.
[26] M. Zheng, G.C. Dismukes, Biochemistry 35 (1996) 8955.